Finite Time Convergence Incremental Nonlinear Dynamic Inversion-Based Attitude Control for Flying—Wing Aircraft with Actuator Faults

Shaojie Zhang *, Wuhan Han and Yuemei Zhang

College of Automation Engineering, Nanjing University of Aeronautics and Astronautics, Nanjing 211106, China; han_wuhan@careri.com (W.H.); 13856599834@163.com (Y.Z.)

* Correspondence: zhangsj@nuaa.edu.cn

check for updates

Abstract: In this paper, a two-loop fault-tolerant attitude control scheme is proposed for flying-wing aircraft with actuator faults. A regular nonlinear dynamic inversion (NDI) control is used in the outer attitude loop, and a finite time convergence incremental nonlinear dynamic inversion (FINDI) control combined with control allocation strategy is used in the inner angular rate loop. Prescribed performance bound (PPB) is designed to constrain the tracking errors within a residual set, so the prescribed system performance can be guaranteed. An optimal anti-windup (AW) compensator is introduced to solve the actuator saturation problem. Simulation results demonstrate the effectiveness of the proposed approach.

Keywords: flying-wing aircraft; fault-tolerant control; finite time convergence incremental nonlinear dynamic inversion; prescribed performance bound; control allocation; anti-windup control

1. Introduction

The flying-wing aircraft has received wide research in recent years for its light weight, good stealth and high control surfaces efficiency [1–3]. However, the aerodynamic configuration of flying-wing aircraft brings new challenges for aircraft control. The flying-wing aircraft has bad longitudinal stability and maneuverability because of the short moment arm. There is no vertical tail in flying-wing aircraft; this leads to bad lateral stability. In aircrafts, there are more control actuators than controlled variables to achieve multiple control objectives and high performance; the maneuverability becomes flexible but control surfaces become coupled after introducing the elevons and drag rudders for flying-wing aircrafts. Therefore, many approaches have been designed to improve the control performance of flying-wing aircrafts.

Several nonlinear control approaches have been proposed to overcome the shortcomings of traditional linearization approaches [4–10]; one popular approach is nonlinear dynamic inversion (NDI) control. NDI control eliminates the nonlinearities in the aircraft system by state feedback, then the nonlinear model is transformed into a linear one controlled by a virtual linear input. The control performance of NDI, however, depends on accurate mathematical models of the plants, which makes it strongly influenced by model uncertainties and the robustness of the controller cannot be guaranteed. An alternative solution to make the controller less dependent on the model is implicit NDI proposed by [11] in 1990; this concept was later further developed into incremental nonlinear dynamic inversion (INDI). Compared to NDI, instead of modeling the angular acceleration based on the state and inverting the aircraft model to get the control input, a desired increment in measured angular acceleration is introduced into an increment of the control input to control the aircraft system. Therefore, INDI is inherently implicit in the sense that desired closed-loop dynamics do not reside in some explicit model

to be followed. This way, any unmodeled dynamics are measured and compensated, which increases the robustness of the nonlinear system.

In most of the present papers, the measured angular acceleration is assumed to be readily available; this is, however, hard to be obtained in reality. In addition, the time delay problem always arises in angular acceleration feedback. A proposed method to deal with the time delay problem is combining INDI with a linear predictive filter to predict the angular acceleration [12]. However, the prediction requires additional modeling and it cannot predict disturbances. The authors of [13,14] apply the concept of finite time convergence to INDI, called FINDI; it does not focus on the way angular acceleration is acquired in a timely manner, but solves the time delay problem by the convergence of the tracking error between reference signal and closed-loop output.

Fault-tolerant capability [15,16] is an important feature for safety-critical systems, and hardware redundancy is a key ingredient in fault-tolerant systems, which can be seen in the modern military and civil aircrafts. In order to improve the reliability of the system, fault-tolerant control (FTC) should be introduced in the controller design. With the increase in the available redundant actuators in the flying-wing aircraft, how to distribute the control signals to these actuators is known as the control allocation problem [17]. In the case of actuator fault or failure, an effective control allocation of the actuators is needed to make the faulty actuators be compensated by the remaining healthy actuators, so that the acceptable performance is achieved without redesigning the control low. Therefore, the FINDI based on reasonable control allocation can greatly improve the fault-capability of flying-wing aircraft.

Besides the nonlinear control law and fault-tolerant capability, another important issue associated with the flight control system concerns the transient state performance. The designed controller is expected to achieve the requirement of prescribed system performance in the actual flight control systems [18]. The traditional method is adjusting parameters of the PID controller. However, with the increase in system performance index, the aforementioned method fails to meet multiple performance requirements simultaneously. In the control system, the state performance of the control system can be transferred into the constraint problem of tracking error performance. Traditionally, the nonlinear controller is designed to guarantee that the tracking error is converged to a residual set whose size depends on design parameters and some bounded though unknown terms [19–21]. However, no systematic procedure exits to accurately compute the required upper bounds, thus making the a priori selection of the design parameters to satisfy certain steady state behavior practically impossible. Moreover, the convergence rate is difficult to be established even in the case of known nonlinearities [22]. Until recently, such issues were discussed only in terms of the norm of the tracking error that is derived to be a function of explicit design parameters and initial estimation errors [23,24]. However, the aforementioned performance index is connected only indirectly with the actual system response. Therefore, in this work, regarding performance it is required that the tracking error converges to a predefined arbitrarily small residual set with convergence rate no less than a certain prespecified value. The prescribed performance controller has been proposed in [25–27] for specific classes of affine nonlinear systems. In [28], it is proposed that the prescribed performance bound (PPB)-based method to restrain the convergence rate of the tracking error and the transient performance of the system is improved. If the PPB system is stable, the tracking errors will be within the prescribed error bounds all the way through. In [29], a command filtered adaptive backstepping compensation approach based on PPB is proposed for the flying-wing aircraft system with actuator stuck or loss of effectiveness and achieves some good results.

In flight control systems, physical limitations of actuators have to be considered. Large control signals for high performance demanded systems are inevitable, which will cause the actuators' saturation with their own performance constraints. The control efficiency will be discounted and the stability of closed-loop system cannot be guaranteed in the presence of saturation. The control strategies to solve the problem of actuators' saturation in the nonlinear system can be divided into two kinds: the direct method [30,31] and the anti-windup (AW) method [32–35]. The control law of the direct method is found based on the Lyapunov theory and optimal control theory. It considers the

performance index of a nonlinear system to design the controller, then the optimal performance of the system is guaranteed. However, the direct method is too complex and often has additional restrictions for the nonlinear system. Compared to the direct method, the AW method adds the compensator to the nonlinear control system. In addition, the control input of the AW compensator is based on the error between the normal control input and control saturated input. Therefore, the compensator works only when the control signals are in the saturation zone. For the AW scheme, the control performance with actuators' saturation is improved while reducing the complexity of the nonlinear control system. As one of the AW methods, the Internal-Model-Control (IMC) type compensator scheme is studied for nonlinear input affine systems by using a state-dependent saturation function in [32,33]. In [34], the control performance is guaranteed by introducing a general AW compensator into the NDI control system based on the optimal IMC theorem.

In this paper, a new PPB-FINDI method with control allocation is proposed for the attitude tracking control of flying-wing aircraft with multiple actuator faults; the fault-tolerant capability of the nonlinear system is improved. In addition, a novel AW scheme is introduced into the PPB-FINDI control system to compensate the actuator saturations.

The structure of this paper is as follows: Section 2 briefly reviews the theorems of NDI, INDI and FINDI. The nonlinear model of flying-wing aircraft is discussed in Section 3. Section 4 proposes the specific design of the FINDI controller based on PPB and control allocation. Section 5 introduces an AW scheme into the PPB-FINDI control system. Finally, simulation results are given by MATLAB in Section 6.

2. NDI, INDI and FINDI

Consider a nonlinear control-affined system

$$\dot{x} = F(x) + G(x)u \tag{1}$$

$$y = H(x) \tag{2}$$

where $x \in \mathbb{R}^{n_x}$ is state vector, $u \in \mathbb{R}^{n_u}$ is input vector, $y \in \mathbb{R}^{n_y}$ is output vector, $F(x)$, $G(x)$ and $H(x)$ are smooth nonlinear functions, and for $\forall x \in \mathbb{R}^{n_x}$, $H(x) \neq 0$.

Assumption 1. $\|G(x)\|$ and $\|G(x)\|\|G(x)\|^{-1}$ are both bound for $\forall x \in \mathbb{R}^{n_x}$.

Remark 1. *Assumption 1 can guarantee $G(x)$ is non-singular.*

The derivative of Equation (2) is given by

$$\dot{y} = \frac{dH(x)}{dt} = \frac{\partial H(x)}{\partial x}\frac{dx}{dt} = \nabla H(x)\dot{x} = \nabla H(x)(F(x) + G(x)u)$$
$$= \nabla H(x)F(x) + \nabla H(x)G(x)u = L_f H(x) + L_g H(x)u \tag{3}$$

In Equation (3), $L_f H(x) = \nabla H(x) f(x)$ is the first-order Lie derivative along the function $F(x)$, $L_g H(x)$ is the first-order Lie derivative along the function $G(x)$. Assume that $L_g H(x)$ is not zero and the relationship between y and u is established by NDI theory in Equation (3). Then, NDI control law can be designed to transform the dynamic characteristics of the nonlinear system into linear dynamic characteristics through Equation (4), where $\dot{y}$ is replaced by the pseudocontrol input v.

$$u = L_g H(x)^{-1}(v - L_f H(x)) \tag{4}$$

The pseudocontrol input v is a signal tracked by the derivative of the output. Consequently, the output can be controlled by an appropriate design of v that is usually obtained by a linear

controller, depending on the error e between the reference signal and closed-loop output. It is shown as Equation (5), where LC denotes the linear controller to be designed.

$$v = (\text{LC})e \tag{5}$$

In this paper, we consider that $H(x) = x$ in Equation (2), and it should be noted that $x \neq 0$ herein. Then Equation (4) can be rewritten as

$$u = G^{-1}(x)(v - F(x)) \tag{6}$$

Substituting Equation (6) into Equation (1), we can get the linear control law as

$$\dot{x} = v \tag{7}$$

NDI control depends on $F(x)$ and $G(x)$ to eliminate the nonlinearities in the aircraft system. However, if model uncertainties exist, the exact elimination of nonlinearities becomes impossible. Considering the uncertainties $\Delta F(x)$ and $\Delta G(x)$, Equation (1) can be described as

$$\dot{x} = F(x) + \Delta F(x) + (G(x) + \Delta G(x))u \tag{8}$$

Substituting Equation (6) into Equation (8), then

$$
\begin{aligned}
\dot{x} &= F(x) + \Delta F(x) + (G(x) + \Delta G(x))(G^{-1}(x)(v - f(x))) \\
&= \Delta F(x) - \Delta G(x)G^{-1}(x)F(x) + (I + \Delta G(x)G^{-1}(x))v
\end{aligned}
\tag{9}
$$

where I denotes the identity matrix. As it can be seen, the linear control law $\dot{x} = v$ is satisfied only for $\Delta F(x) = \Delta G(x) = 0$. Otherwise, the closed-loop system is not linearized anymore. This drawback is the main motivation to develop a more robust version of the NDI, known as INDI.

Compared to NDI, INDI control calculates the increment of the control input for each sampling time, instead of computing the total control input directly. In order to obtain the incremental form of the system, Equation (1) is rewritten by first-order Taylor series expansion.

$$\dot{x} \approx \dot{x}_0 + \left. \frac{\partial}{\partial x}(F(x) + G(x)u) \right|_{\substack{x = x_0 \\ u = u_0}} (x - x_0) + \left. \frac{\partial}{\partial u}(F(x) + G(x)u) \right|_{\substack{x = x_0 \\ u = u_0}} (u - u_0) + \Delta_{\text{H.O.T}} \tag{10}$$

where x_0 and u_0 denote x and u in the previous control step in the discrete implementation. The zero-order term of the Taylor series $\dot{x}_0$ is obtained from sensor that satisfies Equation (11). $\Delta_{\text{H.O.T}}$ is the higher order term. Under high update frequency, the value of higher order term $(x - x_0)^k, k \geq 2$ is small enough to be ignored, and its influence on the control effect can be neglected. Hence $\Delta_{\text{H.O.T}}$ is neglected here.

$$\dot{x}_0 = F(x_0) + G(x_0)u_0 \tag{11}$$

For short time increments and a sufficiently high control update rate, x approaches x_0, that is $x - x_0 \approx 0$. As a result, Equation (10) becomes

$$\dot{x} \approx \dot{x}_0 + G(x)(u - u_0) \tag{12}$$

Replacing $\dot{x}$ by the pseudocontrol input v, the linearizing control input is shown by inverting Equation (12). With Assumption 1, the INDI control law can be designed as

$$u = u_0 + G^{-1}(x)(v - \dot{x}_0) \tag{13}$$

Comparing Equations (6) and (13), the control law in INDI does not depend on F, changes in F are reflected in $\dot{x}_0$ and the effectiveness of INDI controller is dependent on the measurements of $\dot{x}_0$ and u_0.

Assuming ideal measurements, all the model uncertainties lie in G (uncertainties in F are reflected in $\dot{x}_0$). Considering the uncertainties $\Delta G(x)$, Equation (12) can be described as

$$\dot{x} \approx \dot{x}_0 + (G(x) + \Delta G(x))(u - u_0) \tag{14}$$

Substituting Equation (13) into (14), then

$$\begin{aligned} \dot{x} &= \dot{x}_0 + (G(x) + \Delta G(x))(G^{-1}(x)(v - \dot{x}_0)) \\ &= -\Delta G(x)G^{-1}(x)\dot{x}_0 + (I + \Delta G(x)G^{-1}(x))v \end{aligned} \tag{15}$$

In INDI control, $\dot{x}$ approaches $\dot{x}_0$ with high control update rate and Equation (15) can be rewritten as

$$(I + \Delta G(x)G^{-1}(x))\dot{x} \approx (I + \Delta G(x)G^{-1}(x))v \Rightarrow B\dot{x} \approx Bv \tag{16}$$

where $B = I + \Delta G(x)G^{-1}(x)$. Therefore, $\dot{x} \approx v$ still holds, which means that uncertainties in the control matrix G do not affect the INDI control; robust control design is not needed in this case.

Most research results assume that $\dot{x}_0$ is obtained by an ideal sensor without time delay. However, the time delay will affect the availability of $\dot{x}_0$, then the output will be affected too. In this paper, the FINDI control is designed to converge the error in finite time and eliminate the influence of the time delay.

Based on the finite time convergence theorem [36], the pseudocontrol input v is obtained by a non-smooth controller in Equation (17) combined with a reference differential signal, shown in Equation (18)

$$G_n : v_n = K|x_r - x|^\sigma \cdot sign(x_r - x) \tag{17}$$

$$v = v_n + \dot{x}_r \tag{18}$$

where G_n denotes the non-smooth controller that can resist disturbance and v_n denotes the output of G_n. x_r denotes the reference signal and $\dot{x}_r$ is feed forward control. K denotes the bandwidth gain that satisfies $K > 0$. σ is a constant and $\sigma \in (0, 1]$ is satisfied. Based on the theorem in [14], the pseudocontrol input v obtained from Equation (18) is used for the INDI control law, then the tracking error will converge to zero in finite time.

Remark 2. *Equations (17) and (47) in the flying-wing aircraft control are typical finite time control schemes; the anti-disturbance ability and convergence speed are obviously better than smooth feedback control. Although the response smoothness is a bit lower than continuous control, it is acceptable in the simulation of this paper. If there is obvious chattering, we can use the proposed method in [37] to cope with it.*

3. Aircraft Model

The configuration of the flying-wing aircraft is shown in Figure 1; two engines are installed on both sides of the blended body symmetrically. All the control surfaces of aircraft are set behind a serrated double "W" wing, including one pair of drag rudders, one pair of ailerons, one pair of elevons and one pair of elevators. All the deflections of control surfaces are in their mechanical limitations; ailerons, elevators and elevons in $-25° \sim +25°$, drag rudders in $0° \sim \pm 90°$.
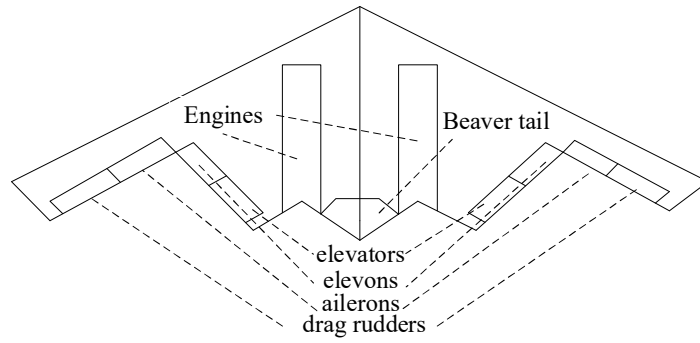
Figure 1. Configuration of flying-wing aircraft.

The mathematical model of the flying-wing aircraft is given as

$$\dot{x} = F + Gu \tag{19}$$

where $x = [\mu\ \alpha\ \beta\ p\ q\ r]^T$, μ denotes kinematic roll angle and α, β denote attack angle and sideslip angle, respectively. p, q, r denote roll, pitch and yaw rates along the body axis. $u = [u_a\ u_e\ u_r]^T$, u_a, u_e, u_r denote the deflections of ailerons, elevators and rudders, respectively.

NDI control needs the control matrix $G(x)$ to be non-singular, which means the number of input variables must be same as the state variables. Consequently, the time scale separation principle is introduced to divide the flying-wing aircraft nonlinear model into two loops; the outer loop with Equation (20) and the inner rate loop with Equation (21).

$$\dot{x}_1 = F_1(x_1, x_2) = f_1 + g_1 x_2 \tag{20}$$

$$\dot{x}_2 = F_2(x_2, u) = f_2 + g_2 u \tag{21}$$

$$y = x_1 \tag{22}$$

where $x_1 = [\mu\ \alpha\ \beta]^T$ is the state vector of attitude control and $x_2 = [p\ q\ r]^T$ is the state vector of angular rate control.

x_1 and x_2 are described as

$$\begin{bmatrix} \dot{p} \\ \dot{q} \\ \dot{r} \end{bmatrix} = I^{-1}(\begin{bmatrix} \overline{L}_A \\ M_A + M_T \\ N_A \end{bmatrix} - \begin{bmatrix} p \\ q \\ r \end{bmatrix} \times I \begin{bmatrix} p \\ q \\ r \end{bmatrix}) \tag{23}$$

$$\begin{bmatrix} \dot{\mu} \\ \dot{\alpha} \\ \dot{\beta} \end{bmatrix} = \begin{bmatrix} \cos\alpha\cos\beta & 0 & \sin\alpha \\ \sin\beta & 1 & 0 \\ \sin\alpha\sin\beta & 0 & -\cos\alpha \end{bmatrix}^{-1} \cdot (-T_{VB}{}^T \begin{bmatrix} -\dot{\chi}\sin\gamma \\ \dot{\gamma} \\ \dot{\chi}\cos\gamma \end{bmatrix} + \begin{bmatrix} p \\ q \\ r \end{bmatrix}) \tag{24}$$

where $I = \begin{bmatrix} I_{xx} & -I_{xy} & -I_{xz} \\ -I_{xy} & I_{yy} & -I_{yz} \\ -I_{xz} & -I_{yz} & I_{zz} \end{bmatrix}$ denotes the moment of inertia matrix, and $I_{xy} = I_{yz} = I_{xz} = 0$ in this paper. $\overline{L}_A$, M_A, N_A are the aerodynamic pitching, rolling and yawing moments along the body axis, M_T is the thrust moment brought by the power of engines, and these moments are denoted as

$$\overline{L}_A = (C_{l_\beta}\beta + C_{l_{u_a}}u_a + C_{l_{u_r}}u_r + C_{l_{\overline{p}}}\overline{p} + C_{l_{\overline{r}}}\overline{r})QS_wb \tag{25}$$

$$M_A = (C_{m_0} + C_{m_\alpha}\alpha + C_{m_{\overline{\dot{\alpha}}}}\overline{\dot{\alpha}} + C_{m_{\overline{q}}}\overline{q} + C_{m_{u_e}}u_e)QS_wc_A \tag{26}$$

$$N_A = (C_{n_\beta}\beta + C_{n_{u_a}}u_a + C_{n_{u_r}}u_r + C_{n_{\overline{p}}}\overline{p} + C_{n_{\overline{r}}}\overline{r})QS_wb \tag{27}$$

$$M_T = z_T T_{\max} u_{th} \tag{28}$$

where $\bar{p} = \frac{pb}{2V}, \bar{q} = \frac{qc_A}{2V}, \bar{r} = \frac{rb}{2V}, \bar{\dot{\alpha}} = \frac{\dot{\alpha}c_A}{2V}$ denote the dimensionless roll angular rate, pitch angular rate, yaw angular rate and attack angular rate, respectively. b denotes the wind chord and c_A denotes the wing mean geometric chord. $Q = \frac{1}{2}\rho V^2$ denotes the kinetic pressure where ρ denotes the air density and V denotes the air speed. S_w denotes the reference area of the wing. $C_{l_\beta}, C_{l_{u_a}}, C_{l_{u_r}}, C_{l_{\bar{p}}}, C_{l_{\bar{r}}}, C_{m_0}, C_{m_\alpha}, C_{m_{\bar{\alpha}}}, C_{m_{\bar{q}}}, C_{m_{u_e}}, C_{n_\beta}, C_{n_{u_a}}, C_{n_{u_r}}, C_{n_{\bar{p}}}$ and $C_{n_{\bar{r}}}$ denote the aerodynamic derivatives of $\bar{L}_A, M_A$ and N_A. $T_{\max}$ denotes the maximum thrust of one engine, u_{th} denotes the total throttle angle of two engines and z_T is a constant of the z-axis. T_{VB} denotes the transformation matrix from body axis to velocity axis. γ and χ denote the fight path angle and kinematic azimuth angle.

In aircraft model, g_1, f_1, g_2, f_2 are

$$g_1 = \begin{bmatrix} \cos\alpha\cos\beta & 0 & \sin\alpha \\ \sin\beta & 1 & 0 \\ \sin\alpha\sin\beta & 0 & -\cos\alpha \end{bmatrix}^{-1} \tag{29}$$

$$f_1 = \begin{bmatrix} \cos\alpha\cos\beta & 0 & \sin\alpha \\ \sin\beta & 1 & 0 \\ \sin\alpha\sin\beta & 0 & -\cos\alpha \end{bmatrix}^{-1} \cdot (-T_{VB}{}^T \begin{bmatrix} -\dot{\chi}\sin\gamma \\ \dot{\gamma} \\ \dot{\chi}\cos\gamma \end{bmatrix}) \tag{30}$$

$$g_2 = \begin{bmatrix} \frac{\partial\dot{p}}{\partial u_a} & \frac{\partial\dot{p}}{\partial u_e} & \frac{\partial\dot{p}}{\partial u_r} \\ \frac{\partial\dot{q}}{\partial u_a} & \frac{\partial\dot{q}}{\partial u_e} & \frac{\partial\dot{q}}{\partial u_r} \\ \frac{\partial\dot{r}}{\partial u_a} & \frac{\partial\dot{r}}{\partial u_e} & \frac{\partial\dot{r}}{\partial u_r} \end{bmatrix} = QS_w \begin{bmatrix} \frac{C_{l_{u_a}}}{I_{xx}} & 0 & \frac{C_{l_{u_r}}}{I_{xx}} \\ 0 & \frac{C_{m_{u_e}}}{I_{yy}} & 0 \\ \frac{C_{n_{u_a}}}{I_{zz}} & 0 & \frac{C_{n_{u_r}}}{I_{zz}} \end{bmatrix} \begin{bmatrix} b \\ c_A \\ b \end{bmatrix} \tag{31}$$

$$f_2 = \dot{x}_2 - g_2 u$$
$$= \begin{bmatrix} \left[(I_{yy} - I_{zz})qr + QS_w b(C_{l_\beta}\beta + \frac{b(C_{l_{\bar{p}}}\bar{p} + C_{l_{\bar{r}}}\bar{r})}{2V}) \right]/I_{xx} \\ \left[z_T T_{\max} u_{th} - (I_{xx} - I_{zz})pr + QS_w c_A(C_{m_0} + C_{m_\alpha}\alpha + \frac{c_A(C_{m_{\bar{\alpha}}}\bar{\dot{\alpha}} + C_{m_{\bar{q}}}\bar{q})}{2V}) \right]/I_{yy} \\ \left[(I_{xx} - I_{yy})pq + QS_w b(C_{n_\beta}\beta + \frac{b(C_{n_{\bar{p}}}\bar{p} + C_{n_{\bar{r}}}\bar{r})}{2V}) \right]/I_{zz} \end{bmatrix} \tag{32}$$

4. Attitude Control Law Design

4.1. PPB Theory

In this paper, prescribed performance means that the closed-loop output tracking error converges to a predefined residual set with convergence rate no less than a certain prespecified value.

Considering a scalar tracking error $e(t), \forall t \geq 0$, the prescribed performance $\mathcal{F}$ can be defined as

$$\mathcal{F} = \left\{ (t,e) \in \mathbb{R}_{t\geq 0} \times \mathbb{R} \middle| \varphi_0^-(t) < e(t) < \varphi_0^+(t) \right\} \tag{33}$$

where $\varphi_0^-(t)$ and $\varphi_0^+(t)$ denote prescribed performance functions satisfying

(1) $\varphi_0^-(t)$ and $\varphi_0^+(t)$ are smooth.
(2) $\varphi_0^-(t), \varphi_0^+(t)$ and their n-order derivative are bounded.
(3) $\lim_{t\to\infty}\varphi_0^-(t) = \varphi^-, \lim_{t\to\infty}\varphi_0^+(t) = \varphi^+$, where φ^- and φ^+ denote prescribed constants and $\varphi^- < \varphi^+$.

If $\varphi_0^-(t) = -\underline{\zeta}\varepsilon(t), \varphi_0^+(t) = \bar{\zeta}\varepsilon(t)$, then $\mathcal{F}$ can be transformed into

$$\mathcal{F} = \left\{ (t,e) \in \mathbb{R}_{t\geq 0} \times \mathbb{R} \middle| -\underline{\zeta}\varepsilon(t) < e(t) < \bar{\zeta}\varepsilon(t) \right\} \tag{34}$$

where $0 < \underline{\zeta}, \overline{\zeta} \le 1$, $\varepsilon(t)$ is the smooth performance function to be designed and the decreasing function satisfying $0 < \lim\limits_{t\to\infty} \varepsilon(t) = \varepsilon_\infty < \varepsilon_0 = \lim\limits_{t\to 0} \varepsilon(t)$. Assume that $\varepsilon(t) = (\varepsilon_0 - \varepsilon_\infty)e^{-\lambda t} + \varepsilon_\infty$, where ε_0, ε_∞ and λ are prescribed positive constants. $\overline{\zeta}\varepsilon_\infty$ denotes the upper bound of prescribed steady-state error and $\underline{\zeta}\varepsilon_\infty$ denotes the lower bound. If $e(t) > 0$, $\overline{\zeta}$ times of the decreasing rate of $\varepsilon(t)$ is the lower bound of the decreasing rate of $e(t)$. The maximum overshoot of $e(t)$ is less than $\overline{\zeta}\varepsilon_0$. If $e(t) < 0$, $\underline{\zeta}$ times of the decreasing rate of $\varepsilon(t)$ is the lower bound of the decreasing rate of $e(t)$. The maximum overshoot $e(t)$ is bigger than $\underline{\zeta}\varepsilon_0$.

Then, if $e(t)$ satisfies Equation (34) under the designed control law, the tracking error will converge to $-\underline{\zeta}\varepsilon_\infty < \lim\limits_{t\to\infty} e(t) = \overline{\zeta}\varepsilon_\infty$. For tracking errors of different variables, different prescribed performance functions can be chosen according to the system performance requirements.

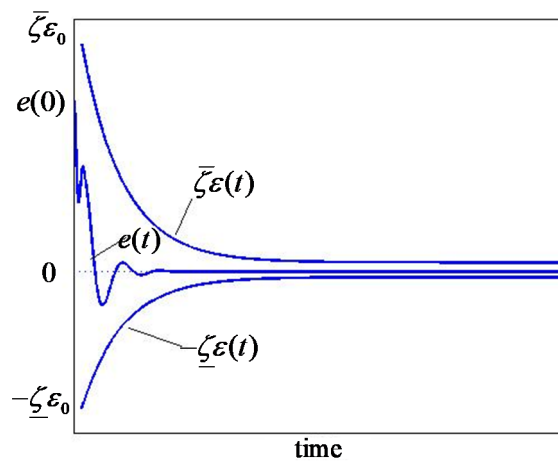The PPB of the tracking error is shown as Figure 2.

Figure 2. Prescribed performance bound of the tracking error.

Design an increasing scalar function $J(w)$ to satisfy Equations (35) and (36), where w denotes the transformed tracking error.

$$-\underline{\zeta} < J(w) < \overline{\zeta} \tag{35}$$

$$\lim\limits_{w\to-\infty} J(w) = -\underline{\zeta}, \ \lim\limits_{w\to+\infty} J(w) = \overline{\zeta}, J(0) = 0 \tag{36}$$

Then, if $e(t)$ satisfies Equation (37), $e(t)$ can satisfy Equation (34).

$$e(t) = \varepsilon(t)J(w) \tag{37}$$

In this paper, $J(w)$ is designed as

$$J(w) = \frac{\overline{\zeta}e^{(w+z)} - \underline{\zeta}e^{-(w+z)}}{e^{(w+z)} + e^{-(w+z)}} \tag{38}$$

$$z = (\ln(\underline{\zeta}/\overline{\zeta}))/2 \tag{39}$$

It can be proved that $J(w)$ satisfies Equations (35) and (36). Then, w can be designed as

$$w = \frac{1}{2}\ln(\overline{\zeta}\varsigma(t) + \overline{\zeta}\underline{\zeta}) - \frac{1}{2}\ln(\overline{\zeta}\underline{\zeta} - \underline{\zeta}\varsigma(t)) \tag{40}$$

$$\varsigma(t) = \frac{e(t)}{\varepsilon(t)} = J(w) \tag{41}$$

Differentiating Equation (40), it follows that

$$\dot{w} = \frac{\partial J^{-1}}{\partial \varsigma} \dot{\varsigma} = \xi(\dot{e} - \frac{e\dot{\varsigma}}{\varsigma}) \tag{42}$$

$$\xi = \frac{1}{2\varsigma}(\frac{1}{\varsigma + \underline{\varsigma}} - \frac{1}{\varsigma - \overline{\varsigma}}) \tag{43}$$

where $\dot{e}$ is the scalar differential tracking error.

4.2. Outer Loop Control

In the outer loop, there is no model uncertainty, so NDI can be used to design the controller. There are three state items μ, α and β in the outer loop and we make the PPB transformation separately. Noting the tracking error of the outer loop as $e_1 = \begin{bmatrix} e_\mu & e_\alpha & e_\beta \end{bmatrix}^T$, then we use Equations (40) and (41) to transform it into the PPB transformed error of outer loop, denoted by $w_1 = \begin{bmatrix} w_\mu & w_\alpha & w_\beta \end{bmatrix}^T$. Hence, Equation (5) can be rewritten as

$$v_1^w = (LC)w_1 \tag{44}$$

where $v_1^w = \begin{bmatrix} v_\mu^w & v_\alpha^w & v_\beta^w \end{bmatrix}^T$ is the new pseudocontrol input based on the PPB transformation.

Therefore, the standard NDI controller, based on Equations (6), (20), (29) and (30), is given as

$$x_2^r = g_1^{-1}(v_1^w - f_1) = \begin{bmatrix} \cos\alpha\cos\beta & 0 & \sin\alpha \\ \sin\beta & 1 & 0 \\ \sin\alpha\sin\beta & 0 & -\cos\alpha \end{bmatrix} \begin{bmatrix} v_\mu^w \\ v_\alpha^w \\ v_\beta^w \end{bmatrix} + T_{VB}{}^T \begin{bmatrix} -\dot{\chi}\sin\gamma \\ \dot{\gamma} \\ \dot{\chi}\cos\gamma \end{bmatrix} \tag{45}$$

where $x_2^r = [p_r \ q_r \ r_r]^T$ is the reference angular rate signal that is used as the input of the inner loop, and the control diagram is shown as Figure 3.
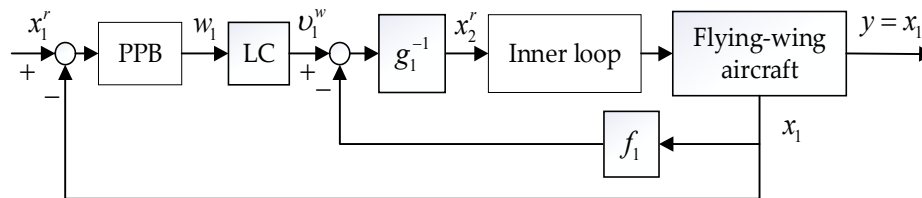

Figure 3. Outer loop control.

4.3. Inner Loop Control

With model uncertainties and time delay in the inner loop, FINDI is used to design the controller.

There are three states (p, q, r) in the inner loop and we make the PPB transformation separately. Noting the tracking error of the inner loop as $e_2 = \begin{bmatrix} e_p & e_q & e_r \end{bmatrix}^T$, then we use Equations (40) and (41) to transform it into the PPB transformed error of the inner loop, denoted by $w_2 = \begin{bmatrix} w_p & w_q & w_r \end{bmatrix}^T$. Hence, Equation (17) can be rewritten as

$$v_n^w = K|w_2|^\sigma \cdot sign(w_2) \tag{46}$$

where v_n^w denotes the new output of non-smooth controller based on the PPB transformation.

Therefore, the FINDI controller, based on Equations (13), (18), (21) and (31), is given as

$$u = u_0 + g_2^{-1}(v_n^w + \dot{x}_2^r - \dot{x}_2^0) = \begin{bmatrix} u_a^0 \\ u_e^0 \\ u_r^0 \end{bmatrix} + (QS_w \begin{bmatrix} \frac{C_{l_{u_a}}}{I_{xx}} & 0 & \frac{C_{l_{u_r}}}{I_{xx}} \\ 0 & \frac{C_{m_{u_e}}}{I_{yy}} & 0 \\ \frac{C_{n_{u_a}}}{I_{zz}} & 0 & \frac{C_{n_{u_r}}}{I_{zz}} \end{bmatrix} \begin{bmatrix} b \\ c_A \\ b \end{bmatrix})^{-1} \cdot (K \begin{bmatrix} w_p \\ w_q \\ w_r \end{bmatrix}^\sigma \cdot sign(\begin{bmatrix} w_p \\ w_q \\ w_r \end{bmatrix}) + \begin{bmatrix} \dot{p}_r \\ \dot{q}_r \\ \dot{r}_r \end{bmatrix} - \begin{bmatrix} \dot{p}_0 \\ \dot{q}_0 \\ \dot{r}_0 \end{bmatrix}) \tag{47}$$

In Equation (47), $\dot{x}_2^0 = \begin{bmatrix} \dot{p}_0 & \dot{q}_0 & \dot{r}_0 \end{bmatrix}^T$ and $\dot{x}_2^r = \begin{bmatrix} \dot{p}_r & \dot{q}_r & \dot{r}_r \end{bmatrix}^T$ can be calculated by using different approaches. In this paper, they are obtained by the following washout filter.

$$sZ(s) = \frac{s\omega_n^2}{s^2 + 2\delta_n\omega_n + \omega_n^2} \tag{48}$$

where ω_n denotes the natural angular frequency of the filter and δ_n denotes the damping ratio of the filter. $u_0 = \begin{bmatrix} u_a^0 & u_e^0 & u_r^0 \end{bmatrix}^T$ is obtained by $Z(s)$.

$$Z(s) = \frac{\omega_n^2}{s^2 + 2\delta_n\omega_n + \omega_n^2} \tag{49}$$

In Equation (47), it is obvious that the term $\dot{x}_2^r - \dot{x}_2^0$ is the differential tracking error of the inner loop, denoted by $\dot{e}_2 = \begin{bmatrix} \dot{e}_p & \dot{e}_q & \dot{e}_r \end{bmatrix}^T$. Then, we can use Equations (42) and (43) to transform it into the PPB-transformed differential error of the inner loop, denoted by $\dot{w}_2 = \begin{bmatrix} \dot{w}_p & \dot{w}_q & \dot{w}_r \end{bmatrix}^T$. Hence, Equation (47) can be rewritten as

$$
\begin{aligned}
u &= u_0 + g_2^{-1}(v_n^w + \dot{w}_2) = u_0 + g_2^{-1}v_2^w \\
&= \begin{bmatrix} u_a^0 \\ u_e^0 \\ u_r^0 \end{bmatrix} + (QS_w \begin{bmatrix} \frac{C_{l_{u_a}}}{I_{xx}} & 0 & \frac{C_{l_{u_r}}}{I_{xx}} \\ 0 & \frac{C_{m_{u_e}}}{I_{yy}} & 0 \\ \frac{C_{n_{u_a}}}{I_{zz}} & 0 & \frac{C_{n_{u_r}}}{I_{zz}} \end{bmatrix} \begin{bmatrix} b \\ c_A \\ b \end{bmatrix})^{-1} \cdot (K \begin{Vmatrix} w_p \\ w_q \\ w_r \end{Vmatrix}^\sigma \cdot sign(\begin{bmatrix} w_p \\ w_q \\ w_r \end{bmatrix}) + \begin{bmatrix} \dot{w}_p^r \\ \dot{w}_q^r \\ \dot{w}_r^r \end{bmatrix} - \begin{bmatrix} \dot{w}_p^0 \\ \dot{w}_q^0 \\ \dot{w}_r^0 \end{bmatrix})
\end{aligned} \tag{50}
$$

$$v_2^w = v_n^w + \dot{w}_2 \tag{51}$$

Considering the actuator faults, fault-tolerant control should be designed for the system. The flying-wing aircraft with redundancy configuration control actuators can be designed through the control allocation strategy, so that the control signal can be allocated to each operation surface reasonably and effectively. Moreover, the control effect of the actuator fault can be compensated.

Partial loss of effectiveness and stuck types of actuator faults are considered in this paper. We note u_{al}, u_{ar}, u_{el1}, u_{el2}, u_{er1}, u_{er2}, u_{rl} and u_{rr} as the deflections of left aileron, right aileron, left elevator, left elevon, right elevator, right elevon, left and right drag rudders of the flying-wing aircraft, respectively. The control allocation without actuator fault can be shown as Equation (52).

$$
\begin{aligned}
&u_a = (u_c)_{al} - (u_c)_{ar}, (u_c)_{al} = -(u_c)_{ar} = 0.5 \cdot u_a \\
&u_e = (u_c)_{el1} + (u_c)_{el2} + (u_c)_{er1} + (u_c)_{er2}, (u_c)_{el1} = (u_c)_{el2} = (u_c)_{er1} = (u_c)_{er2} = 0.25 \cdot u_e \\
&u_r = (u_c)_{rl} + (u_c)_{rr}, rank(diag[(u_c)_{rl}, (u_c)_{rr}]) = 1
\end{aligned} \tag{52}
$$

where $(u_c)_{al}$, $(u_c)_{ar}$ $(u_c)_{el1}$, $(u_c)_{el2}$, $(u_c)_{er1}$, $(u_c)_{er2}$, $(u_c)_{rl}$ and $(u_c)_{rr}$ denote the deflections of aforementioned control surfaces without fault, u_c is the fault-free actuator. The control allocation scheme without actuator fault is shown in Figure 4.

The control allocation scheme is able to adjust at any time according to different faults. Suppose that the left aileron loses its 40% efficiency and the left elevator is stuck at K_s. Equation (52) can be rewritten as Equation (53), and the deflections of $u = [u_a \ u_e \ u_r]^T$ can maintain stability.

$$
\begin{aligned}
&u_a = 0.6 \cdot (u_c)_{al} - (1 + 0.4) \cdot (u_c)_{ar}, (u_c)_{al} = -(u_c)_{ar} = 0.5 \cdot u_a \\
&u_e = (\frac{(u_c)_{el2} - K_s}{3} + (u_c)_{el1}) + K_s + (\frac{(u_c)_{el2} - K_s}{3} + (u_c)_{er1}) \\
&\quad + (\frac{(u_c)_{el2} - K_s}{3} + (u_c)_{er2}), (u_c)_{el1} = (u_c)_{el2} = (u_c)_{er1} = (u_c)_{er2} = 0.25 \cdot u_e \\
&u_r = (u_c)_{rl} + (u_c)_{rr}, rank(diag[(u_c)_{rl}, (u_c)_{rr}]) = 1
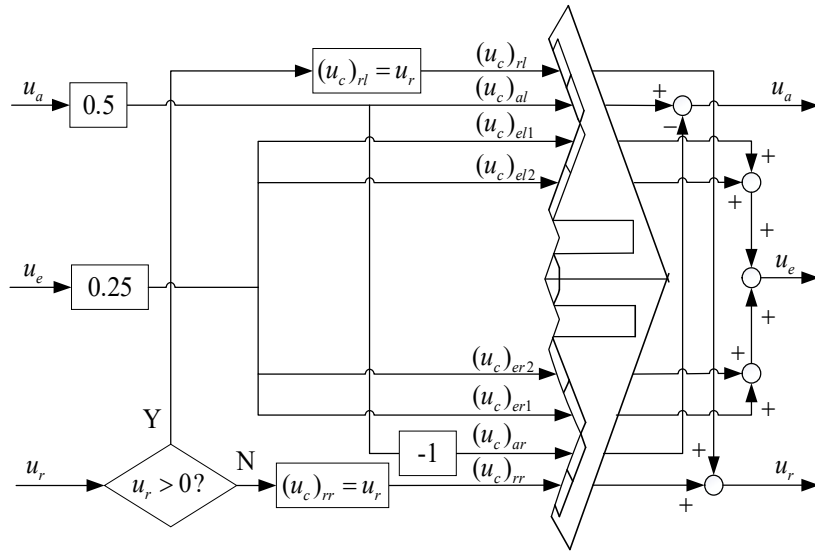\end{aligned} \tag{53}
$$

Figure 4. Control allocation without actuator fault.

5. Attitude Control with Anti-Windup Scheme

When there are saturations in the actuators, the saturation function and dead zone function in the actuators are noted as

$$u_s = sat(u) \tag{54}$$

$$\psi(u) = u - u_s \tag{55}$$

So Equation (21) can be rewritten as

$$\dot{x}_2 = f_2 + g_2 u_s \tag{56}$$

Assumption 2. *System (56) is open-loop exponentially stable for $r > 0$, $\|x_2\| \le r$; that is, when $u_s = 0$, the origin of $\dot{x}_2 = f_2$ is exponentially stable.*

Remark 3. *Assumption 2 is usually raised to ensure exponential stability of the closed-loop system with input saturations. In aircraft control, it can be achieved by the augmentation system if needed.*

To limit the degradation of tracking performance when saturations occur, a modified AW compensator based on IMC is introduced to the PPB-FINDI control scheme.

The AW compensator is shown as Equations (57)–(59).

$$\dot{x}_2^{AW} = f_2(x_2^{AW}) + g_2(\lambda(x_2^{AW}) - \psi(u)) \tag{57}$$

$$\vartheta_1 = \lambda(x_2^{AW}) + g_2^{-1} f_2(x_2^{AW}) \tag{58}$$

$$\vartheta_2 = x_2^{AW} \tag{59}$$

where $x_2^{AW} \in \mathbb{R}^{n_{x_2}}$ is state vector of the compensator; $\lambda(x_2^{AW})$ is a nonlinear function to be designed; $\vartheta_1 \in \mathbb{R}^{n_u}$ and $\vartheta_2 \in \mathbb{R}^{n_{x_2}}$ are designed to compensate the control input u and output feedback of inner loop x_2.

With consideration of the AW compensator, the PPB-FINDI controller in Equation (50) will be

$$u = u_0 + g_2^{-1}(v_n^w + \dot{w}_2) + \vartheta_1 = u_0 + g_2^{-1} v_2^w + \vartheta_1 \tag{60}$$

$\lambda(x_2^{AW})$ is designed to ensure Equation (61) is exponentially stable when $\psi(u) = 0$.

$$\dot{x}_2^{AW} = f_2(x_2^{AW}) + g_2\lambda(x_2^{AW}) \tag{61}$$

We use the auxiliary linear performance index $d = C_d x$ to design $\lambda(x_2^{AW})$, in which C_d is a constant matrix. Then, according to Theorem 2 in [34], an inequality (62) concerning $\lambda(x_2^{AW})$ is satisfied for $x_2^{AW} \neq 0$ and $\forall x_2$.

$$\begin{bmatrix} \frac{\partial V(x_2^{AW})}{\partial x_2^{AW}}[f(x_2^{AW}) + g_2\lambda(x_2^{AW}) + (x_2^{AW})^T C_d^T C_d x_2^{AW}] & \frac{1}{2}[\frac{\partial V(x_2^{AW})}{\partial x_2^{AW}}g_2 - \lambda^T(x_2^{AW})W] & 0 \\ * & -(W - \frac{\kappa}{2}) & -\frac{1}{2}W \\ * & * & -\eta^2 I \end{bmatrix} < 0 \tag{62}$$

where $V(x_2^{AW}) > 0$ is a Lyapunov function about x_2^{AW}; $W > 0$ is a diagonal matrix; $\kappa > 0$ is a scalar; $\eta \geq 0$ is a constant that denotes $\mathcal{L}_2$-gain of the closed-loop system.

Remark 4. *Theorem 2 in [34] proposes a potential tool for AW compensator design. The design of $\lambda(x_2^{AW})$ can be determined by minimizing η of $\mathcal{L}_2$-gain through the optimal problem.*

Remark 5. *The problem of minimizing η of $\mathcal{L}_2$-gain, subject to inequality (62) is difficult and is unlikely to be convex. $V(x_2^{AW})$ and $\lambda(x_2^{AW})$ are the optimization variables. It is possible to search for them together; however, this would be computationally demanding and ineffective.*

From the practical point of view, we can solve the optimal problem of η by Genetic Algorithms (GAs) [38], then $\lambda(x_2^{AW})$ can be determined by Equations (63) and (64).

$$\lambda(x_2^{AW}) = -g_2^T \frac{\partial V(x_2^{AW})}{\partial x_2^{AW}} \tag{63}$$

$$V(x_2^{AW}) = (x_2^{AW})^T P x_2^{AW} \tag{64}$$

where P is a positive define matrix and the design of $\lambda(x_2^{AW})$ is transformed into the choice of P. It is chosen by the optimal condition of minimizing η of $\mathcal{L}_2$-gain. P is selected as a diagonal matrix based on the genetic and evolutionary principles shown in [39].

6. Simulations

In this section, five simulation studies are given to prove the advantages of the proposed method for flying-wing aircraft. The aircraft parameters are given as $\gamma = 0°$, $\chi = 0°$, $S_w = 16.54$ m^2, $b = 9.44$ m, $c_A = 2.34$ m, $I_{xx} = 6320$ kg·m^2, $I_{yy} = 1010$ kg·m^2, $I_{zz} = 1010$ kg·m^2, $\rho = 0.3639$ kg·m^{-3}, $V = 177$ m·s^{-1} $z_T = -0.117$, $T_{max} = 4900$ N, $u_{th} = 0.3014$, $C_{l_\beta} = -0.000296$, $C_{l_{ua}} = -0.0017$, $C_{l_{ur}} = 0.0006$, $C_{l_{\bar{p}}} = -0.2247$, $C_{l_{\bar{r}}} = 0.1017$, $C_{m_0} = 0.006$, $C_{m_\alpha} = -0.0036$, $C_{m_{\bar{\alpha}}} = -0.1275$, $C_{m_{\bar{q}}} = -5.1447$, $C_{m_{u_e}} = -0.00125$, $C_{n_\beta} = 0.0000236$, $C_{n_{ua}} = 0.000015$, $C_{n_{ur}} = -0.0011$, $C_{n_{\bar{p}}} = -0.0208$, $C_{n_{\bar{r}}} = -0.0045$.

In simulation 1, we compare the control performance of the outer loop between PPB-NDI and regular NDI. The reference signals are $\mu_r = 5\sin(0.75t)$, $\alpha_r = 5\sin(0.75t)$ and $\beta_r = 0°$. The parameters of the PID controller for $x_2 = [\mu \ \alpha \ \beta]^T$ are 20, 0.5, 3; 20, 1, 2; 10, 0.5, 2 and the filter coefficient is 100. The PPB parameters for μ, α and β are $\varepsilon(t) = 1.1e^{(-0.5t)}$, $\underline{\zeta} = 0.2$ and $\overline{\zeta} = 0.3$.

Figures 5 and 6 show the tracking response of μ, α, β. μ and α in Figure 5 can track their desired references. Therefore, the regular NDI controller can guarantee the system performance in μ and α without model uncertainties in the outer loop. In Figure 6, it can be seen that β in the no PPB case does not track the reference signal well. This indicates the effectiveness of the PPB control.
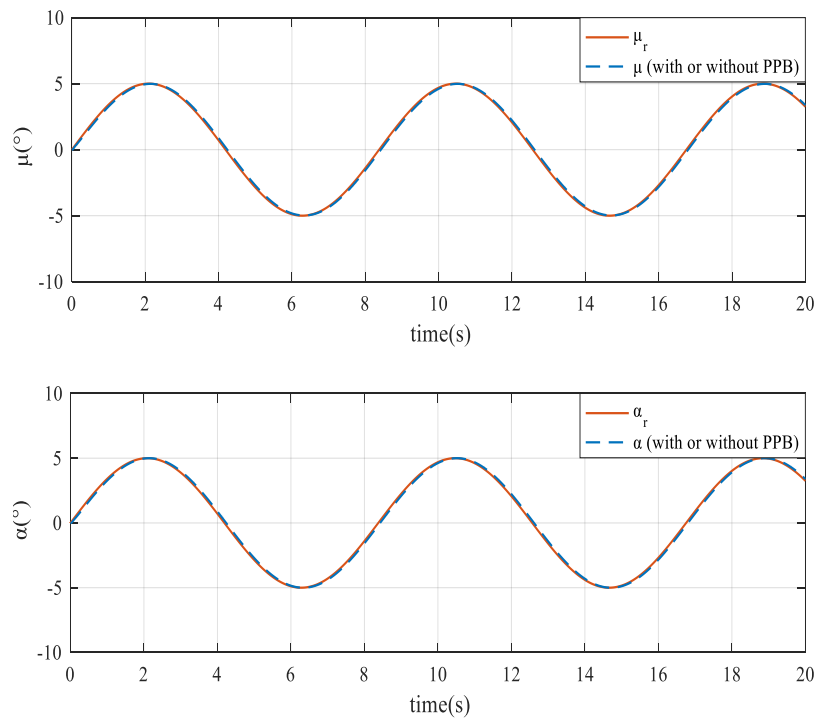
Figure 5. Tracking response of μ and α.
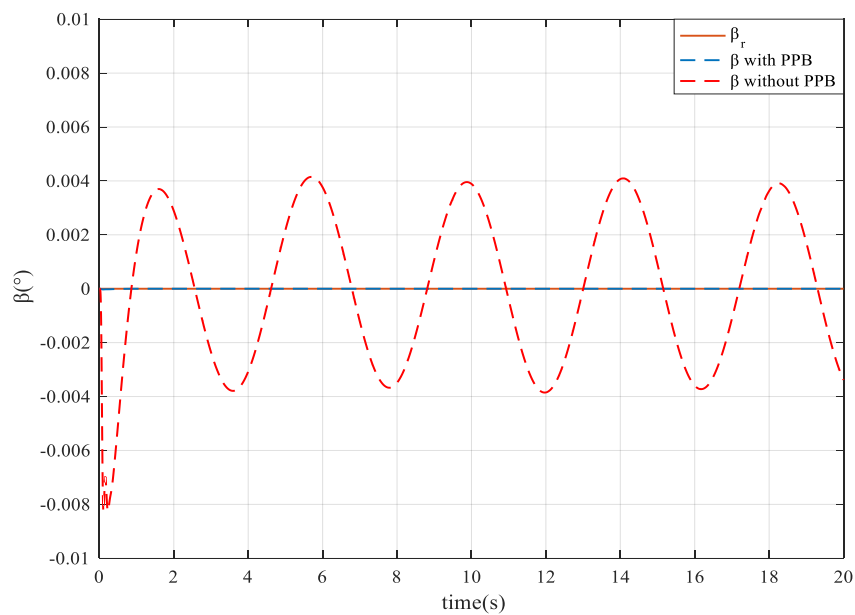

Figure 6. Tracking response of β.

In simulation 2, we compare the performance of inner control between PPB-FINDI and regular FINDI. The reference signals and the PID parameters are the same as simulation 1. The FINDI parameters are $K = 10$, $\sigma = 1$, $Z(s) = \frac{625}{s^2+40s+625}$ and $sZ(s) = \frac{625s}{s^2+40s+625}$. For p, the PPB parameters are chosen as: $\varepsilon_p(t) = 4.4e^{(-t)} + 1.3$, $\underline{\zeta}_p = 0.5$ and $\overline{\zeta}_p = 0.7$. For q, the PPB parameters are chosen as: $\varepsilon_q(t) = 2.4e^{(-t)} + 1.3$, $\underline{\zeta}_q = 0.3$ and $\overline{\zeta}_q = 0.5$. For r, the PPB parameters are chosen as: $\varepsilon_r(t) = 0.22e^{(-t)} + 0.03$, $\underline{\zeta}_r = 0.8$ and $\overline{\zeta}_r = 0.85$.

Figures 7–9 show the tracking response of p, q, r. In Figures 7 and 8, compared with the PPB case, the performance in the no PPB case is worse, especially at the beginning of the simulation. In Figure 9, with the no PPB case, r cannot track the reference well. While in the PPB case, the performance is much

better, the prescribed performance output tracking is achieved. To illustrate the superiority of PPB, Figure 10 shows the tracking error of *r*. The tracking error in the no PPB case is beyond the bound a lot at the beginning of the simulation. In addition, when steady state is reached, the tracking error is still outside the steady-state bound. While in the PPB case, the tracking error is restrained within the bound. In conclusion, by the constraint of PPB, both the transient and steady state performance are improved obviously.
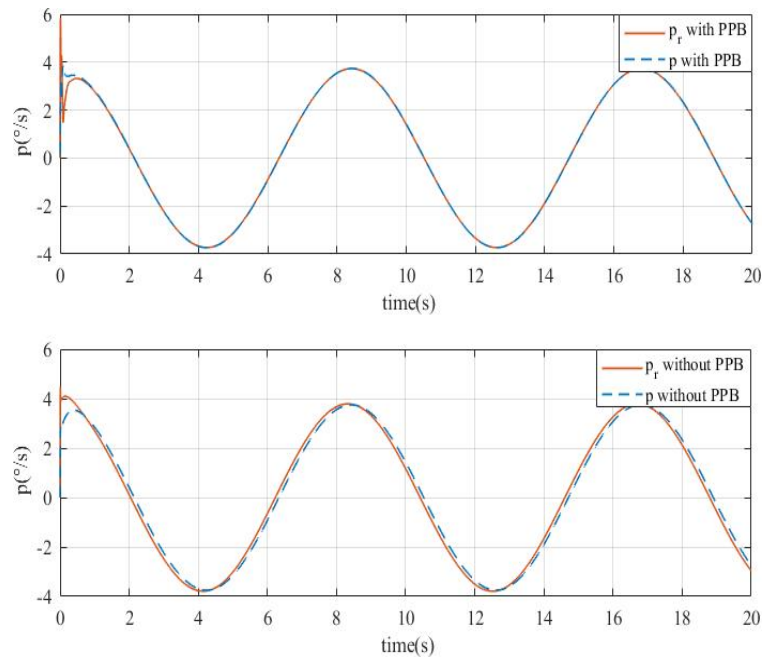
Figure 7. Tracking response of *p*.
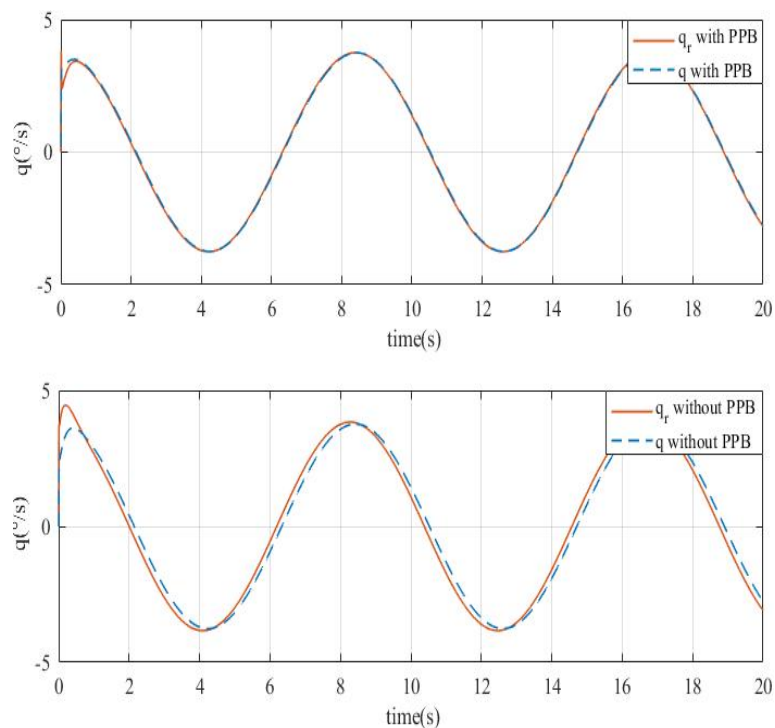
Figure 8. Tracking response of *q*.
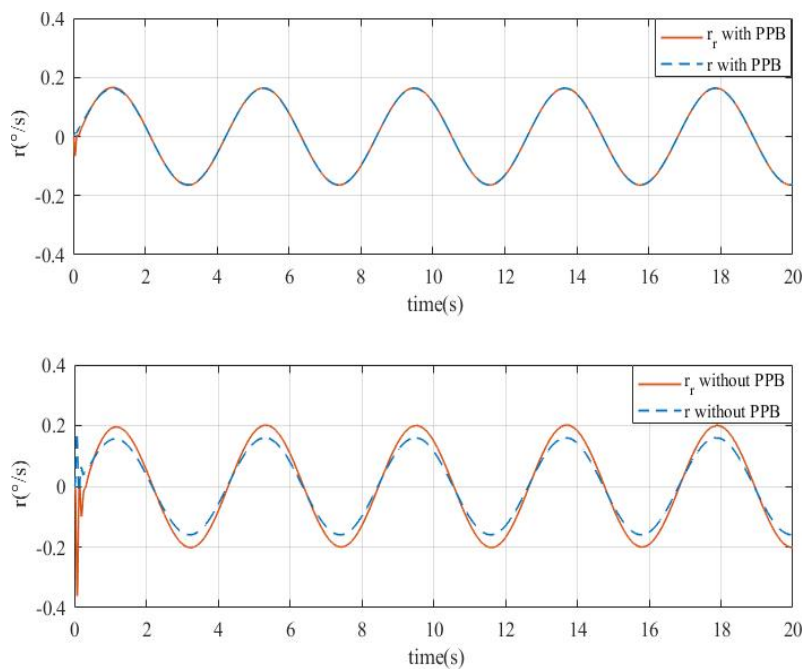
Figure 9. Tracking response of *r*.
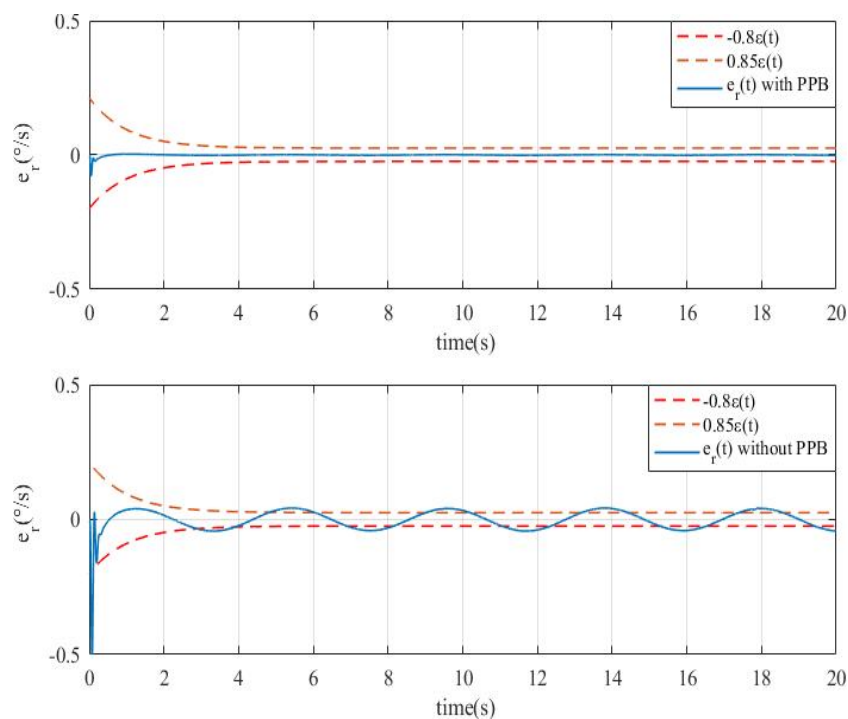
Figure 10. Tracking error of *r*.

In simulation 3, we compare the performance with actuator saturations between the PPB-FINDI combined AW compensator and the PPB-FINDI scheme. The reference signals are $\mu_r = 5\sin(0.2t)$, $\alpha_r = 5\sin(0.2t)$ and $\beta_r = 0$, $P = diag(348.0325,\ 289.0897,\ 76.6576)$; other parameters are the same as simulation 2.

Figures 11 and 12 show the response of $x = [\mu\ \alpha\ \beta\ p\ q\ r]^T$ in two-loop control. In the case of no AW compensator, when there are actuator saturations, the simulation stops in 40 s and the values of some state variables change abruptly (the values of *p* and *r* change into infinity). The system is unstable

without the AW compensator in this simulation, while in the case of AW compensator, the closed-loop output can still follow the reference well when saturations occur. It is obvious that the AW compensator can improve the tracking performance of controllers and solve the actuator saturations problem.
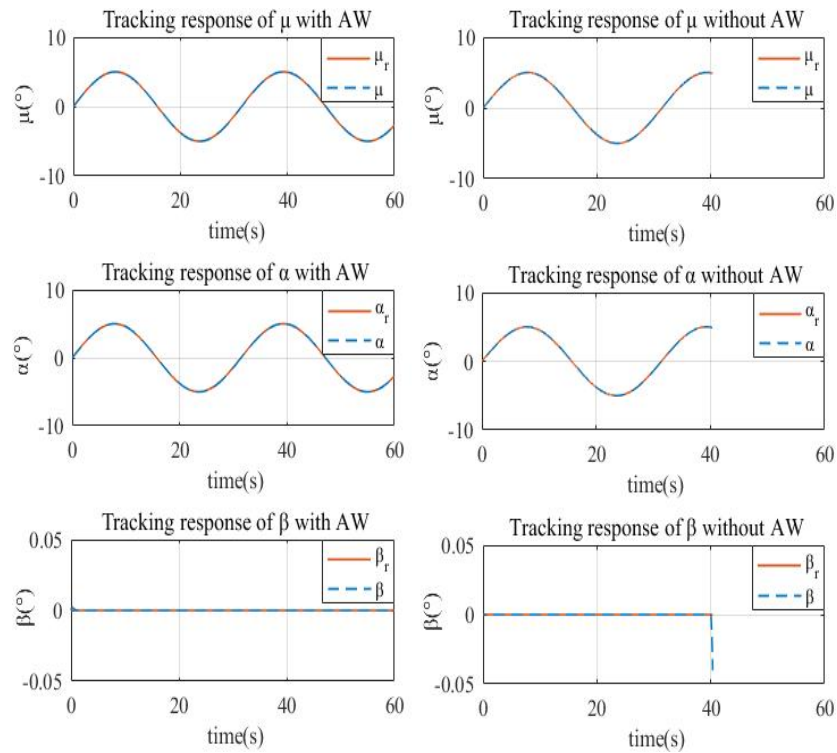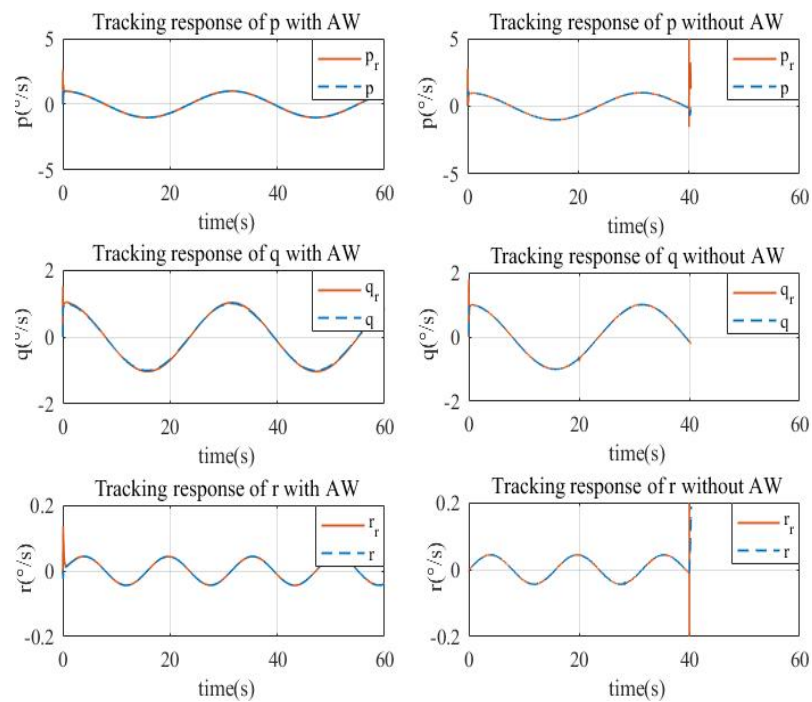
Figure 11. Tracking response μ, α and β.

Figure 12. Tracking response of p, q and r.

In simulation 4, we focus on the compensation of the faulty actuator by control allocation in the inner loop. The reference signals and other control parameters are the same as simulation 3. The faults

of the actuators are: the left elevator is stuck at $-7°$ at 20 s and the right elevator loses its 60% efficiency at 40 s.

Figure 13 shows the deflections of the actuators. It can be seen that when faults occur in an actuator, other actuators will compensate the efficiency lost by the faulty actuator. Figure 14 shows that the control allocation has a good effect in dealing with actuator faults.
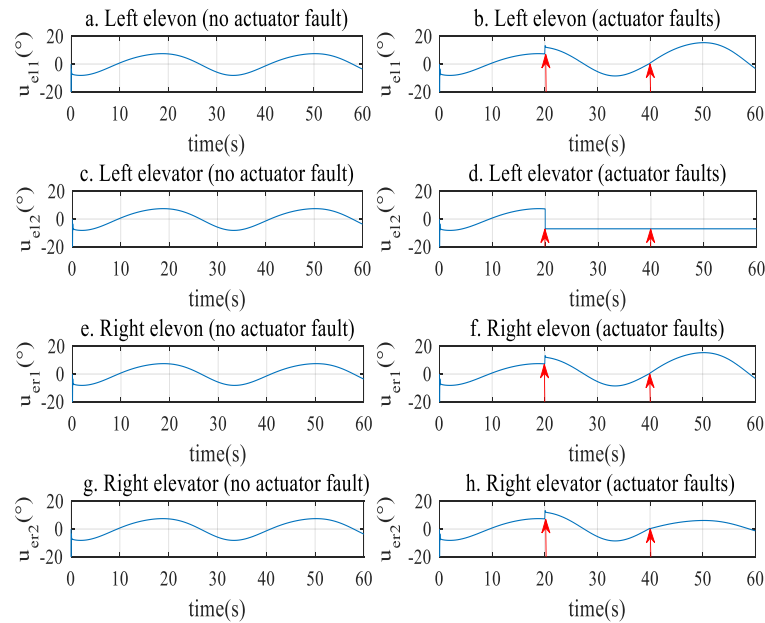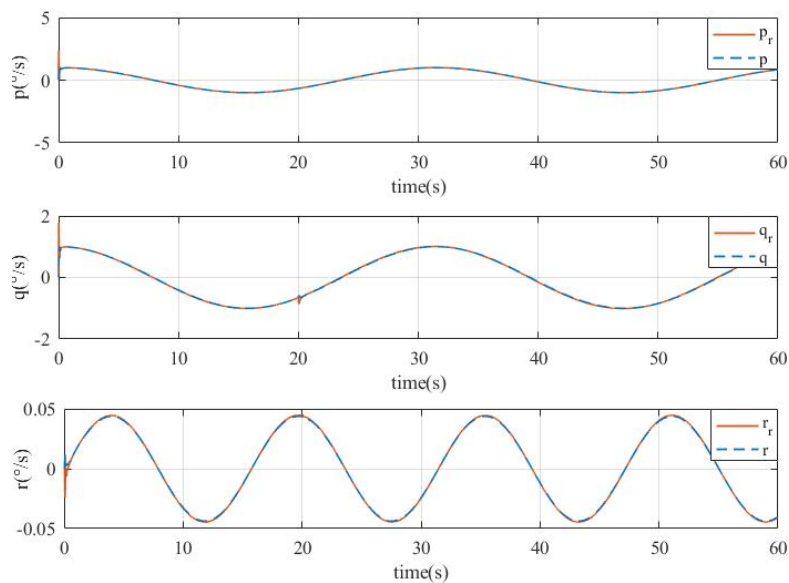

Figure 13. Deflections of the elevons and elevators.

Figure 14. Angular rate tracking with actuator faults.

In simulation 5, we focus on the control characteristics of the proposed method with step inputs. The reference signals are $\mu_r = \begin{cases} 0.1 & t > 0 \\ 0 & t = 0 \end{cases}$, $\alpha_r = \begin{cases} 0.1 & t > 0 \\ 0 & t = 0 \end{cases}$ and $\beta_r = 0°$, t denotes the time. Other control parameters are the same as simulation 4.

Figures 15 and 16 show the case of tracking response without PPB control; we can see that the attitude angles can track the reference inputs, but the overshoots are big, and it is obvious that the tracking errors of angle rates are unacceptably high in the beginning. In Figures 17 and 18,

the outputs can track the reference inputs much better than Figures 15 and 16 because of the PPB control. This indicates the effectiveness of the PPB control with the step inputs.
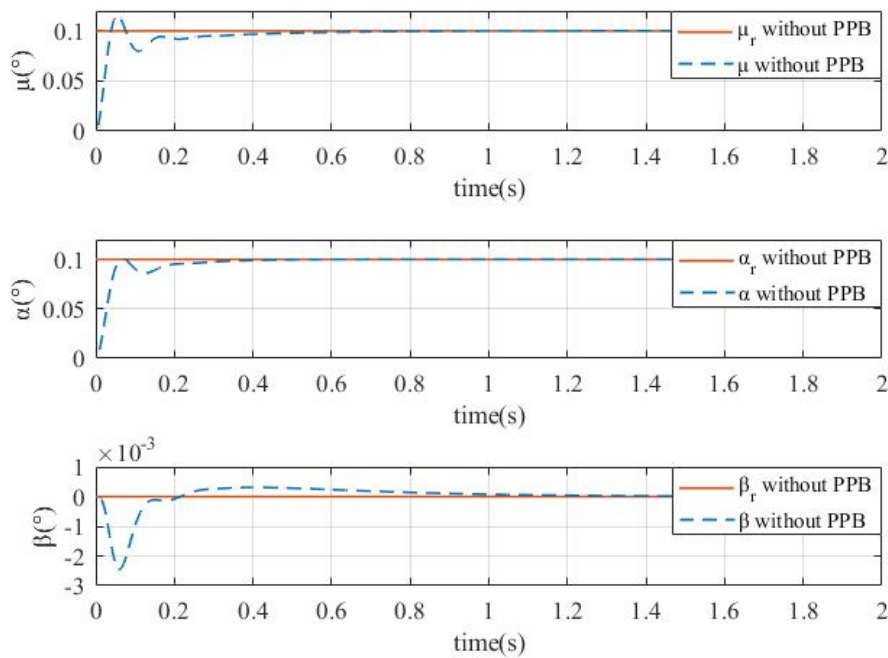

Figure 15. Tracking response of μ, α and β without PPB.
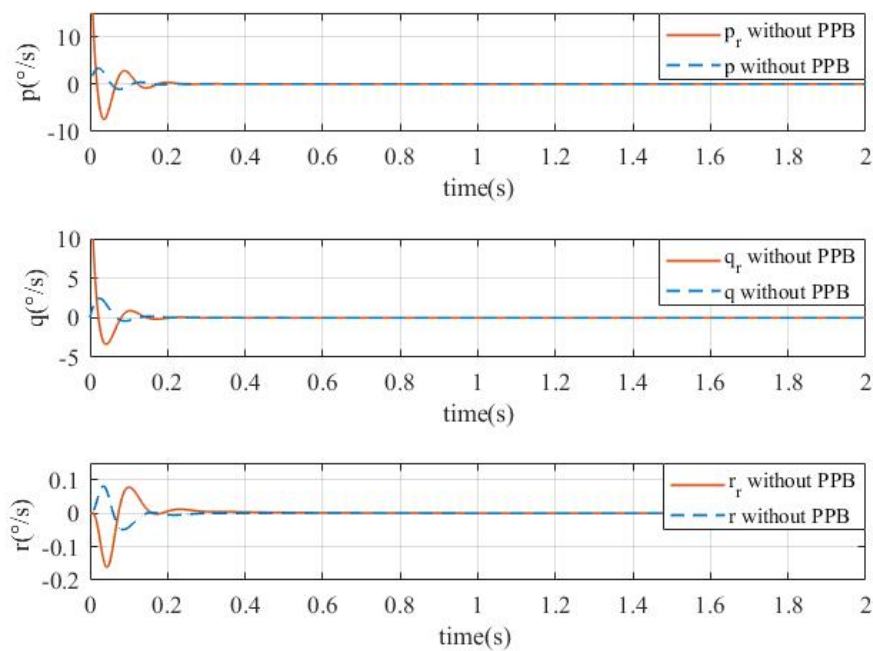

Figure 16. Tracking response of p, q and r without PPB.
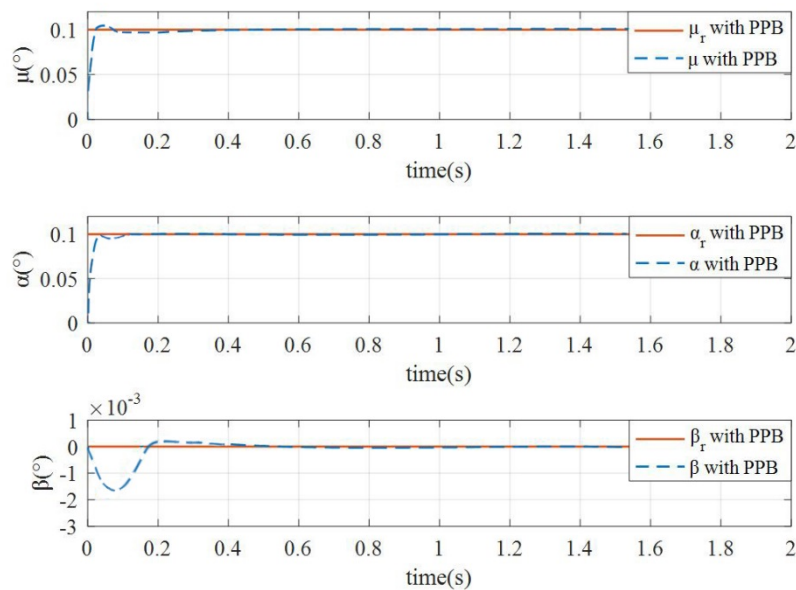
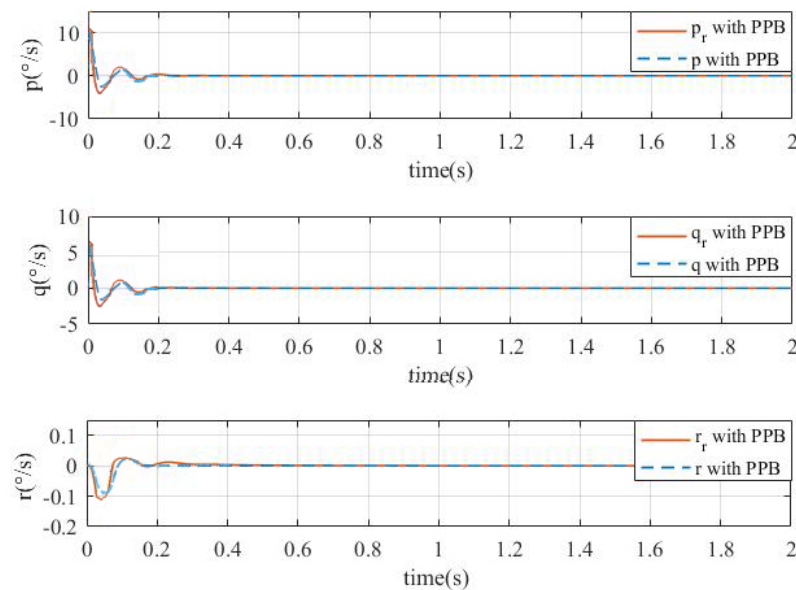**Figure 17.** Tracking response of μ, α and β with PPB.

Figure 18. Tracking response of p, q and r with PPB.

7. Conclusions

The proposed FINDI and NDI flight control laws based on PPB transformation are used in the nonlinear flying-wing aircraft to guarantee transient performance. In addition, optimal IMC-based anti-windup and control allocation schemes are introduced to compensate multiple actuator saturations and faults. Simulation results indicate the validity and effectiveness of the proposed method.

Although the simulation results are quite good in this paper, the proposed method should be tested by flight experiment; hardware in loop simulation will be studied next following the research project schedule. On the other hand, we only consider the attitude control of the flying-wing aircraft in this paper; aircraft position control should be studied next, so there will be two more control loops, the position and flight path control loop, to be considered.

Author Contributions: Funding acquisition, project administration, and writing—review and editing, S.Z.; writing—original draft preparation, W.H. and Y.Z.; Simulations, W.H. All authors have read and agreed to the published version of the manuscript.

Conflicts of Interest: The authors declare no conflict of interest.

References

1. Li, M.; Bai, J.; Li, L.; Meng, X.; Liu, Q.; Chen, B. A gradient-based aero-stealth optimization design method for flying wing aircraft. *Aerosp. Sci. Technol.* **2019**, *92*, 156–169. [CrossRef]
2. Qu, X.; Zhang, W.; Shi, J.; Lyu, Y. A novel yaw control method for flying-wing aircraft in low speed regime. *Aerosp. Sci. Technol.* **2017**, *69*, 636–649. [CrossRef]
3. Voss, A. Open and closed loop gust loads analyses for a flying wing configuration with variable longitudinal stability. *Aerosp. Sci. Technol.* **2019**, *89*, 1–10. [CrossRef]
4. Acquatella, P.; Falkena, W.; Van Kampen, E.-J.; Chu, Q.P. Robust Nonlinear Spacecraft Attitude Control using Incremental Nonlinear Dynamic Inversion. In Proceedings of the American Institute of Aeronautics and Astronautics (AIAA) Guidance, Navigation, and Control Conference, Minneapolis, MN, USA, 13–16 August 2012.
5. Martinez, D.I.; Rubio, J.D.J.; Vargas, T.M.; Garcia, V.; Ochoa, G.; Balcazar, R.; Cruz, D.R.; Aguilar, A.; Novoa, J.F.; Aguilar-Ibanez, C. Stabilization of Robots With a Regulator Containing the Sigmoid Mapping. *IEEE Access* **2020**, *8*, 89479–89488. [CrossRef]
6. Rubio, J.D.J.; Novoa, J.F.; Ochoa, G.; Mújica-Vargas, D.; Garcia, E.; Balcazar, R.; Elias, I.; Cruz, D.R.; Juarez, C.F.; Aguilar, A. Structure Regulator for the Perturbations Attenuation in a Quadrotor. *IEEE Access* **2019**, *7*, 138244–138252. [CrossRef]
7. Alva, J.O.E.; Garcia-Estrada, E.C.; Paramo-Carranza, L.A.; Meda-Campaña, J.A.; Herrera, R.T. Theoretical Application of a Hybrid Observer on Altitude Tracking of Quadrotor Losing GPS Signal. *IEEE Access* **2018**, *6*, 76900–76908. [CrossRef]
8. Rubio, J.D.J.; Martinez, D.I.; Garcia, V.; Gutierrez, G.J.; Vargas, T.M.; Ochoa, G.; Balcazar, R.; Pacheco, J.; Meda-Campaña, J.A.; Mújica-Vargas, D. The Perturbations Estimation in Two Gas Plants. *IEEE Access* **2020**, *8*, 83081–83091. [CrossRef]
9. Aguilar-Ibanez, C.; Suarez-Castanon, M.S. A Trajectory Planning Based Controller to Regulate an Uncertain 3D Overhead Crane System. *Int. J. Appl. Math. Comput. Sci.* **2019**, *29*, 693–702. [CrossRef]
10. Garcia-Sánchez, J.R.; Tavera-Mosqueda, S.; Silva-Ortigoza, R.; Hernández-Guzmán, V.M.; Gutierrez, J.S.; Aranda, M.M.-; Taud, H.; Marciano-Melchor, M. Robust Switched Tracking Control for Wheeled Mobile Robots Considering the Actuators and Drivers. *Sensors* **2018**, *18*, 4316. [CrossRef]
11. Bugajski, D.; Enns, D.; Elgersma, M. A dynamic inversion based control law with application to the high angle-of-attack research vehicle. In Proceedings of the Guidance and Control Conference, American Institute of Aeronautics and Astronautics (AIAA), Portland, OR, USA, 20–22 August 1990; pp. 826–839.
12. Sieberling, S.; Chu, Q.; Mulder, J.A. Robust Flight Control Using Incremental Nonlinear Dynamic Inversion and Angular Acceleration Prediction. *J. Guid. Control Dyn.* **2010**, *33*, 1732–1742. [CrossRef]
13. Zhang, J.; Ding, S.H.; Liu, J.H. Control law design of hypersonic vehicle based on incremental dynamic inverse. *Electron. Opt. Control* **2013**, *20*, 16–20.
14. Su, Z.; Wang, H.; Shao, X. Vehicle attitude control using finite time convergence incremental nonlinear dynamic inversion combined the command differential signals. In Proceedings of the 2014 IEEE Chinese Guidance, Navigation and Control Conference, Yantai, China, 8–10 August 2014; pp. 1079–1084.
15. Liu, S.; Lyu, P.; Lai, J.; Yuan, C.; Wang, B. A fault-tolerant attitude estimation method for quadrotors based on analytical redundancy. *Aerosp. Sci. Technol.* **2019**, *93*, 105290. [CrossRef]
16. Liu, M.; Shao, X.; Ma, G. Appointed-time fault-tolerant attitude tracking control of spacecraft with double-level guaranteed performance bounds. *Aerosp. Sci. Technol.* **2019**, *92*, 337–346. [CrossRef]
17. Waters, S.M.; Voskuijl, M.; Veldhuis, L.L.; Geuskens, F.J. Control allocation performance for blended wing body aircraft and its impact on control surface design. *Aerosp. Sci. Technol.* **2013**, *29*, 18–27. [CrossRef]
18. Zhang, Y.; Wang, S.-H.; Chang, B.; Wu, W.-H. Adaptive constrained backstepping controller with prescribed performance methodology for carrier-based UAV. *Aerosp. Sci. Technol.* **2019**, *92*, 55–65. [CrossRef]

19. Bechlioulis, C.P.; A Rovithakis, G. Prescribed Performance Adaptive Control for Multi-Input Multi-Output Affine in the Control Nonlinear Systems. *IEEE Trans. Autom. Control* **2010**, *55*, 1220–1226. [CrossRef]

20. Bechlioulis, C.P.; Theodorakopoulos, A.; Rovithakis, G.A. Output feedback stabilization with prescribed performance for uncertain nonlinear systems in canonical form. In Proceedings of the 52nd IEEE Conference on Decision and Control, Florence, Italy, 10–13 December 2013; pp. 5084–5089.

21. Li, K.; Wei, Y.; Wang, C.; Deng, H. Longitudinal Attitude Control Decoupling Algorithm Based on the Fuzzy Sliding Mode of a Coaxial-Rotor UAV. *Electronics* **2019**, *8*, 107. [CrossRef]

22. Bechlioulis, C.P.; Rovithakis, G.A. Approximation-free prescribed performance control for unknown SISO pure feedback systems. In Proceedings of the 2013 European Control Conference (ECC), Zurich, Switzerland, 17–19 July 2013; pp. 4544–4549.

23. Ge, S.S.; Hang, C.C.; Lee, T.H.; Zhang, T. *Stable Adaptive Neural Network Control*; Springer Science and Business Media LLC: New York, NY, USA, 2002.

24. Spooner, J.T.; Maggiore, M.; Ordonez, R.; Passino, K.M. *Stable Adaptive Control and Estimation for Nonlinear Systems-Neural and Fuzzy Approximator Techniques*; Wiley: New York, NY, USA, 2002.

25. Bechlioulis, C.P.; Rovithakis, G.A. Adaptive control with guaranteed transient and steady state tracking error bounds for strict feedback systems. *Automatica* **2009**, *45*, 532–538. [CrossRef]

26. Bechlioulis, C.P.; Rovithakis, G.A. Robust Adaptive Control of Feedback Linearizable MIMO Nonlinear Systems with Prescribed Performance. *IEEE Trans. Autom. Control* **2008**, *53*, 2090–2099. [CrossRef]

27. Bechlioulis, C.P.; Rovithakis, G.A. Robust Partial-State Feedback Prescribed Performance Control of Cascade Systems with Unknown Nonlinearities. *IEEE Trans. Autom. Control* **2011**, *56*, 2224–2230. [CrossRef]

28. Bechlioulis, C.P.; Rovithakis, G.A. A low-complexity global approximation-free control scheme with prescribed performance for unknown pure feedback systems. *Automatica* **2014**, *50*, 1217–1226. [CrossRef]

29. Zhang, S.; Shuang, W.; Meng, Q. Control Surface Faults Neural Adaptive Compensation Control for Tailless Flying Wing Aircraft with Uncertainties. *Int. J. Control. Autom. Syst.* **2018**, *16*, 1660–1669. [CrossRef]

30. He, H.; Yan, L.; Tu, J. Guaranteed Cost Stabilization of Time-varying Delay Cellular Neural Networks via Riccati Inequality Approach. *Neural Process. Lett.* **2012**, *35*, 151–158. [CrossRef]

31. Tu, J.; He, H. Guaranteed Cost Synchronization of Chaotic Cellular Neural Networks with Time-Varying Delay. *Neural Comput.* **2012**, *24*, 217–233. [CrossRef] [PubMed]

32. Doyle, F.J., III. An anti-windup input–output linearization scheme for SISO systems. *J. Process Control* **1999**, *9*, 213–220. [CrossRef]

33. Kapoor, N.; Daoutidis†, P. An observer-based anti-windup scheme for non-linear systems with input constraints. *Int. J. Control* **1999**, *72*, 18–29. [CrossRef]

34. Herrmann, G.; Menon, P.P.; Turner, M.C.; Bates, D.G.; Postlethwaite, I. Anti-windup synthesis for nonlinear dynamic inversion control schemes. *Int. J. Robust Nonlinear Control* **2009**, *20*, 1465–1482. [CrossRef]

35. Roos, C.; Biannic, J.-M.; Tarbouriech, S.; Prieur, C.; Jeanneau, M. On-ground aircraft control design using a parameter-varying anti-windup approach. *Aerosp. Sci. Technol.* **2010**, *14*, 459–471. [CrossRef]

36. Ding, S.H.; Li, S.H.; Luo, S. Guidance law design based on continuous finite-time control Technique. *J. Astronaut.* **2011**, *32*, 727–733.

37. Xiao, F.; Wang, L.; Chen, J.; Gao, Y. Finite-time formation control for multi-agent systems. *Automatica* **2009**, *45*, 2605–2611. [CrossRef]

38. Goldberg, D.E. *Genetic Algorithms in Search, Optimization and Machine Learning*; Addison-Wesley: Boston, MA, USA, 1989.

39. Zhang, S.; Meng, Q. An anti-windup INDI fault-tolerant control scheme for flying wing aircraft with actuator faults. *ISA Trans.* **2019**, *93*, 172–179. [CrossRef] [PubMed]